

Abstract: Surface cracks in an ASTM A1011 Nb-HSLA hollow steel beam produced via thin-slab casting were characterized to determine their origin and propagation behavior. Optical microscopy (OM), scanning electron microscopy (SEM), and energy-dispersive X-ray spectroscopy (EDS) revealed intergranular cracking associated with subsurface oxidation. Oxygen enrichment was observed along crack surfaces, while no significant enrichment of copper or other elements typically associated with hot shortness were found. The results suggest that oxide-decorated microcracks formed during high-temperature processing in the bending/straightening region of the caster and subsequently reopened during downstream deformation.

Background & Objectives

Continuous casting solidifies molten steel into slabs that undergo **bending, straightening, reheating, and hot rolling**. This process is typically conducted within a temperature range of 1100°C - 1300°C [1].

Steel exhibits a **low-ductility temperature range** (900°C - 1200°C) in which high temperature embrittlement can lead to defect formation [2]. Oxidation rates in steelmaking increase rapidly around 1000°C -1100°C [3]. Downstream processes impose stress on the steel, under which **fracture** can occur.

Surface hot shortness is embrittlement caused by low melting phases at grain boundaries near the steel/scale interface. This is driven by selective Fe oxidation and subsequent localized elemental enrichment. Hot shortness risk is most prominent when above ~.2 wt% Cu [4]

Intergranular oxidation occurs when elements with a high oxygen affinity (e.g., Si, Mn, Al) oxidize along the steel's grain boundaries [5].

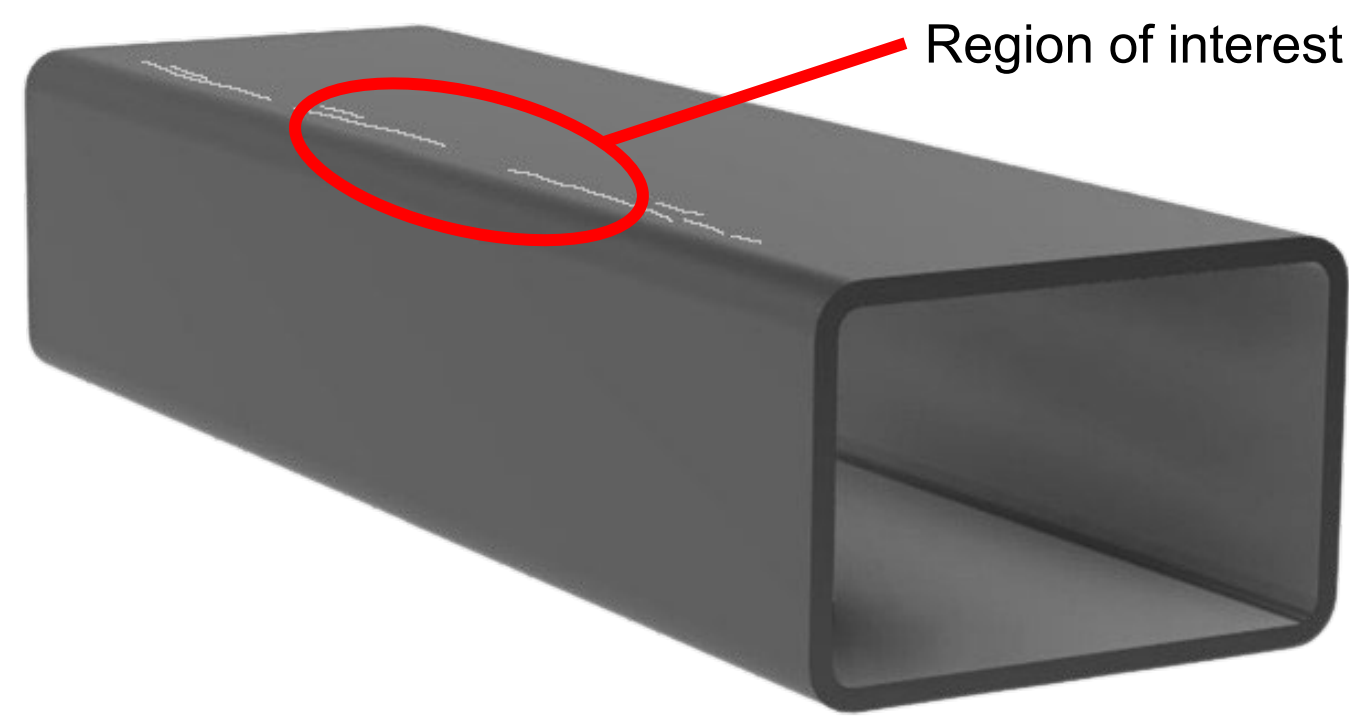


Figure 1. Three-dimensional model of ASTM A1011 steel sample

Objectives

- Identify cause of surface cracks in sponsor's hot rolled steel
- Propose potential mitigation methods to prevent or decrease surface cracking.

Table 1. ASTM A 1011 HSLAS Grade 50 Class 1 steel chemistry

	C (Max%)	Mn (Max%)	P (Max%)	Ni (Max%)	Mo (Max%)	Cu (Max%)
ASTM A1011	0.23	1.35	0.04	0.20	0.06	0.20

Experimental Design

Sectioning

- 20 Specimens were sectioned using a **DoALL 2013-V3 Vertical Band Saw**
 - Specimens were taken from striated and non-striated regions with flat and corner geometries of an ASTM A1011 steel hollow rectangular beam (see Fig.1)

Mounting

- All samples were mounted in Bakelite resin using a **LECO PR4X** mounting press

Grinding & Polishing

- All samples were ground with a **LECO Spectrum System 1000** using silicon carbide (SiC) grit sizes of 400, 600, 800, and 1200
- All samples underwent diamond suspension polishing at 6µm, 3µm, and 1µm
- Following each polishing stage, samples underwent ultrasonic cleaning for 5 minutes in a **Central Machinery Pro. Ultrasonic Cleaner**

Etching

- 5 samples, 1 from each sectioning permutation, were etched with 2% Nital for ~20 seconds

Optical Microscopy (OM)

- Characterization was conducted using an **Olympus SZX7 Optical Microscope**
- Imaging was conducted on etched and unetched samples, with an emphasis on crack morphology
- ImageJ was used for spatial calibration for calculations regarding average crack depth

Scanning Electron Microscopy (SEM) & Energy Dispersive X-ray Spectroscopy (EDS)

- All SEM and EDS was conducted using a **Nanoscience Phenom Desktop SEM**
- SEM micrographs were acquired using backscattered electron (BSE) imaging
- Elemental mapping was conducted at a map resolution of 32-64 pixels with a pixel time of 50ms

Results

Scanning Electron Microscopy (SEM)

- Subsurface precipitates and oxidation were observed near cracks in the samples exhibiting cracking.

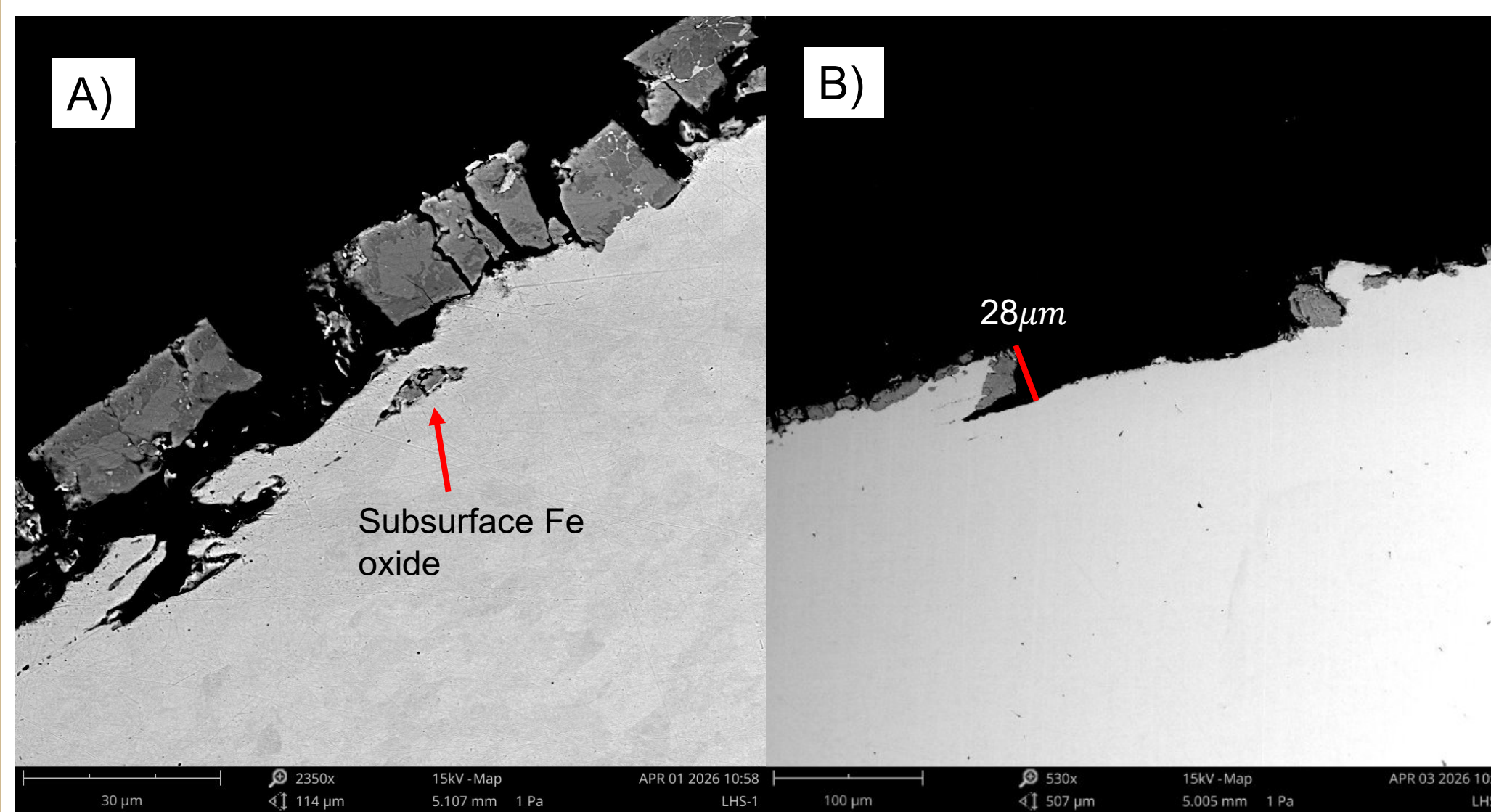


Figure 2. SEM images of the cross-sectional corner region: A) large subsurface oxide, B) crack length annotated for clarity.

Crack Depth

$$D = \left(1 - \frac{R_S - R_D}{R_S}\right) * 100$$

Equation 1: Crack Depth Percentage

R_S = Sample Length
 R_D = Crack Length

$$K_{Ic} = Y\sigma\sqrt{\pi a}$$

Equation 2: Stress Intensity Factor

Y = Geometry Factor
 σ = Applied Stress
 a = Crack Length

Table 2. Summary of Crack Depth Characteristics

Average Crack Depth (%)	Minimum Crack Depth (µm)	Maximum Crack Depth (µm)	Standard Deviation (µm)
0.699	28	68	15.08

Energy Dispersive X-ray Spectroscopy (EDS)

- No significant localized elemental contamination observed near oxidation regions.

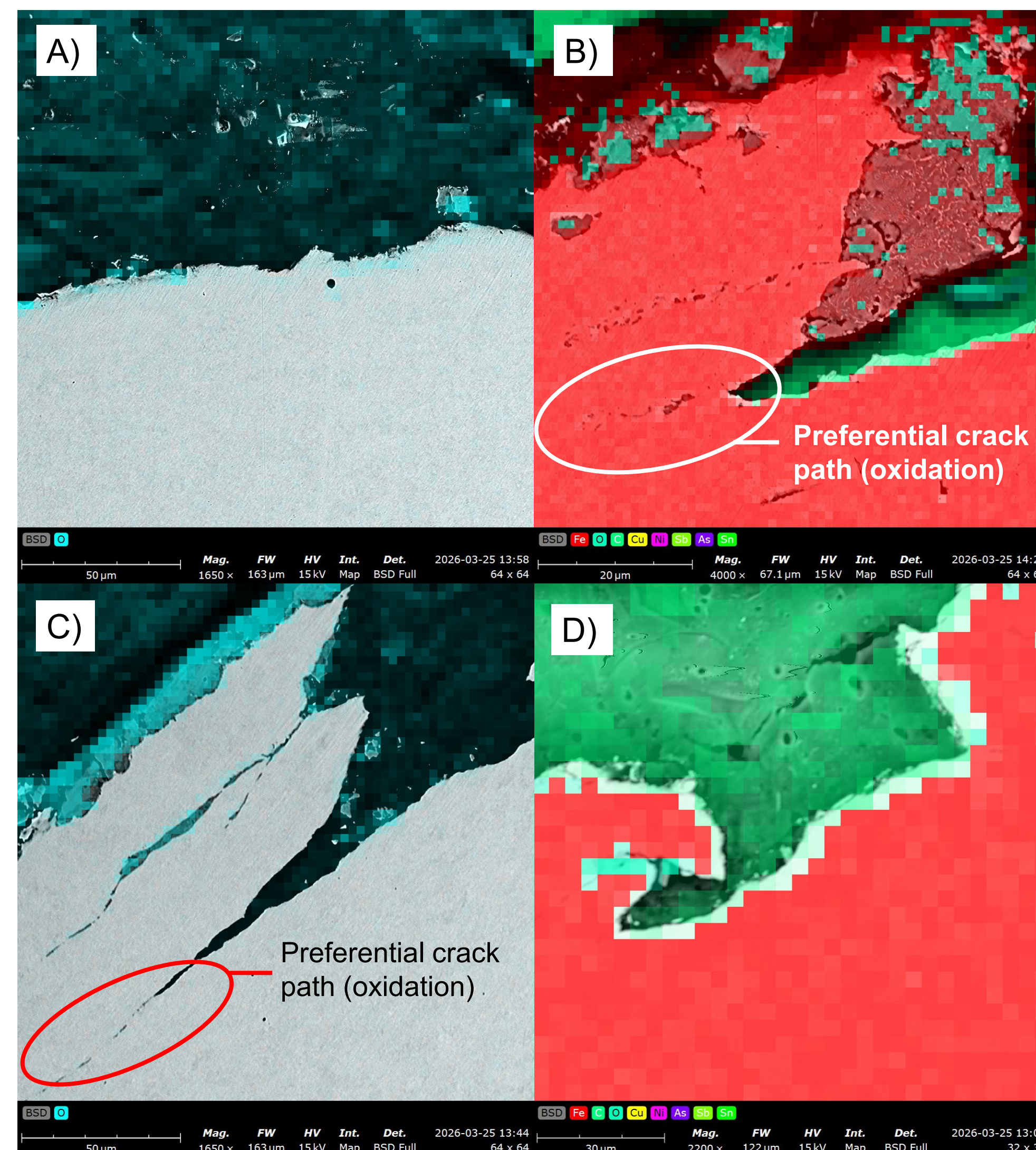


Figure 3. EDS of oxidized cracks: A) Control sample, B) Sample exhibiting subsurface oxidation displaying tramp elements, C) Sample exhibiting subsurface oxidation, D) Sample exhibiting subsurface oxidation showing tramp elements

- Figure 3A) an oxygen mask is overlaid in blue, only surface oxidation is present, no subsurface oxidation is observed
- Figure 3B) oxidation can be observed leading away from the crack laterally. Aluminum Oxide precipitates and oxidation formed below the crack
- Figure 3C) an oxygen mask is overlaid in blue, oxidation can be seen at the surface, in the crack, as well as below the surface of the crack.
- Figure 3D) a mask of tramp elements is overlaid, minor oxidation path can be observed

This work is sponsored by Steel Dynamics, Butler, IN



Discussion

The initial hypothesis related the observed surface cracks to hot shortness; however, this was ruled out due to the **lack of localized low-melting phases** present near the crack regions [4].

EDS revealed the Cu levels throughout the sample were within the allowed tolerance ~.2 wt% and no other low-melting phases were identified. The discolored regions associated with the cracks were identified as Fe oxides.

These observations suggested an alternative cracking mechanism. **Microcracks likely formed after casting, during bending and straightening.** Exposed to a high temperature environment, the cracks oxidized, and were subsequently rolled and 'trapped' subsurface, as seen in Figure 4.

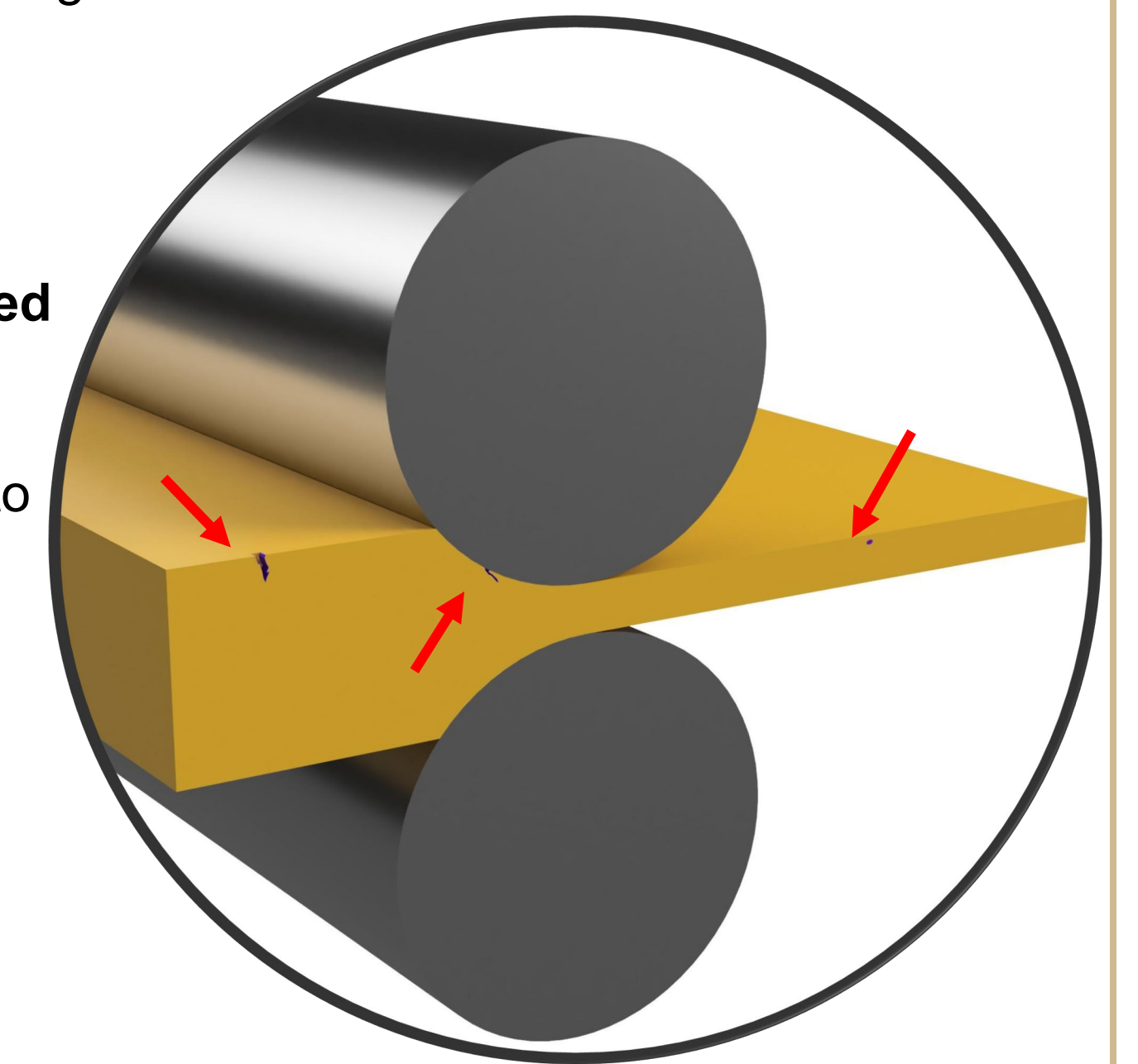


Figure 4. Three-dimensional model of how oxide-decorated microcracks form

The lack of localized high oxygen affinity elements along crack lengths suggested **no intergranular oxidation.**

During downstream deformation, **cracks reopened and propagated along oxidized grain boundaries**, consistent with subsurface oxidation observed along the crack paths in Figures 3B and 3C.

Crack depth has significant implications for steel quality and performance. As crack depth increases, the severity of stress concentration rises, which reduces toughness and structural integrity. Deeper cracks are more likely to enclose oxides and create defects.

Conclusions & Future Work

Conclusions

- Surface cracks in the investigated thin-slab cast steel were characterized using OM, SEM, and EDS.
- Crack morphology indicated oxide-decorated microcracks originating near the steel surface and reopening.
- EDS analysis revealed oxygen enrichment near crack surfaces, indicating oxidation associated with the microcracks.
- No localized copper enrichment was detected, suggesting the defects were unlikely to be caused by copper-induced hot shortness.
- The observed cracks were consistent with oxide-decorated microcracks that likely formed during high-temperature processing and later reopened during deformation.
- These results suggest that oxidation and processing temperature conditions play an important role in crack formation in steel.

Future Work

- Perform higher-resolution SEM and EDS mapping along crack paths to better detect localized elemental variations.
- Repeat testing on additional control and returned samples to improve comparison precision and confidence interval.
- Investigate thermal variations at the sponsors' caster/bender to further evaluate and support the proposed crack mechanism.
- Evaluate the effectiveness of an extended homogenization process in the tunnel furnace at elevated temperatures to eliminate shallow surface cracks through controlled scale formation.
- Analyze the feasibility of a quick cooling process in the continuous casting mold to mitigate thermally straining partially formed microstructures.

References

- Mintz, B., & Crowther, D. N. (2010). Hot ductility of steels and its relationship to the problem of transverse cracking in continuous casting. *International Materials Reviews*, 55(3), 168-196.
- Louhenkilpi, S. (2024). Continuous casting of steel. In *Treatise on process metallurgy* (pp. 343-383). Elsevier.
- Zhang, S., Long, M., Zhang, H., Ai, S., Chen, D., Liu, P., & Duan, H. (2021). Experimental study on evolution of oxidation behavior on high-temperature continuous casting slab surface. *Journal of Materials Research and Technology*, 11, 2049-2058.
- Kapoor, I., Davis, C., & Li, Z. (2021). Effects of residual elements during the casting process of steel production: a critical review. *Ironmaking & steelmaking*, 48(6), 712-727.
- Gaiser, G., Littringer, R., Presoly, P., & Bernhard, C. (2026). The Interaction Between Oxidation-Related Phenomena a Grain Boundaries on Surface Crack Formation in Continuous Casting. *Metallurgical and Materials Transactions B*, 57(2), 963-980.